AMPA receptors gate spine Ca^{2+} transients and spike-timing-dependent potentiation

Niklaus Holbro[1], Åsa Grunditz[1], J. Simon Wiegert, and Thomas G. Oertner[2]

Friedrich Miescher Institute for Biomedical Research, CH-4058 Basel, Switzerland

Edited by Roger A. Nicoll, University of California, San Francisco, CA, and approved August 4, 2010 (received for review April 5, 2010)

Spike timing-dependent long-term potentiation (t-LTP) is the embodiment of Donald Hebb's postulated rule for associative memory formation. Pre- and postsynaptic action potentials need to be precisely correlated in time to induce this form of synaptic plasticity. NMDA receptors have been proposed to detect correlated activity and to trigger synaptic plasticity. However, the slow kinetic of NMDA receptor currents is at odds with the millisecond precision of coincidence detection. Here we show that AMPA receptors are responsible for the extremely narrow time window for t-LTP induction. Furthermore, we visualized synergistic interactions between AMPA and NMDA receptors and back-propagating action potentials on the level of individual spines. Supralinear calcium signals were observed for spike timings that induced t-LTP and were most pronounced in spines well isolated from the dendrite. We conclude that AMPA receptors gate the induction of associative synaptic plasticity by regulating the temporal precision of coincidence detection.

coincidence detection | dendritic spines | caged glutamate | STDP | two-photon imaging

Correlated activity in connected neurons can trigger long-lasting changes in synaptic strength, in which sign and magnitude of synaptic modifications depend on the relative timing of pre- and postsynaptic action potentials (1–3). Presynaptic activity followed by postsynaptic action potentials generally leads to an increase in synaptic strength (timing-dependent long-term potentiation, t-LTP), whereas activity in the reverse order induces long-term depression. Remarkably, the existence of t-LTP was predicted >60 y ago by the Canadian psychologist Donald Hebb as a mechanism for associative learning (4). Although t-LTP is considered a crucial mechanism for activity-dependent modifications of brain circuits, the biophysics of coincidence detection are not fully understood. The required coincidence detector needs to measure the relative timing of postsynaptic action potentials (APs) with respect to the brief glutamate transient in the synaptic cleft with millisecond precision and to convert this temporal measurement into a synapse-specific biochemical signal. Postsynaptic NMDA receptors (NMDARs), due to their sensitivity to both glutamate and membrane depolarization, have been proposed to act as detectors of temporal coincidence. Ca^{2+} influx through NMDARs activates a series of biochemical processes that eventually lead to strengthening of the synaptic connection (5–9). However, there is a striking mismatch between the slow kinetics of NMDARs and the very brief time window in which t-LTP can be induced, suggesting that an additional mechanism is necessary to sharpen the timing sensitivity (10–12).

Here we investigate the role of AMPA receptors (AMPARs) during coincidence detection at Schaffer collateral synapses. Modulation of AMPAR currents during coincident activity strongly affected the induction of synaptic plasticity by pairing of pre- and postsynaptic spikes. Furthermore, we visualized NMDAR-dependent calcium signals in individual spines of CA1 pyramidal cells. During pairing stimulation, AMPAR currents gate NMDARs and precisely regulated the amplitude of postsynaptic Ca^{2+} transients at individual synapses. Interestingly, we found the strongest amplification of Ca^{2+} signals in spines that had a high degree of diffusional isolation from the dendrite, an effect that could be reproduced in a NEURON simulation by changing the diameter of the spine neck. We suggest that amplitude and duration of local, AMPAR-driven excitatory postsynaptic potentials (EPSPs) in spines are critical for coincidence detection with millisecond precision.

Results

Spike Timing-Dependent Potentiation of Schaffer Collateral Synapses. To study the induction of t-LTP, we performed whole-cell patch-clamp recordings from individual hippocampal CA1 pyramidal neurons (Fig. 1*A*). A monopolar glass electrode was positioned close to the recorded cell in *stratum radiatum* to stimulate Schaffer collaterals (Fig. 1*A*). EPSPs were evoked at 0.1 Hz. To induce t-LTP, we paired a single presynaptic stimulation pulse with a brief burst of three back-propagating action potentials (bAPs) at 100 Hz. Pairing was repeated 120 times at 0.2 Hz. When the EPSP preceded the first bAP by Δt = 6 ms, this protocol resulted in reliable and long-lasting potentiation of the synaptic connection (227% ± 20% of baseline, Fig. 1*B*). The magnitude of t-LTP was highly sensitive to the exact timing between pre- and postsynaptic activity (Fig. 1*C*). At Δt = 20 ms, t-LTP was reduced to 144% ± 10% of baseline, and at Δt = 40 ms, no potentiation was observed (95% ± 4%). The NMDAR antagonist dCPP (20 μM) blocked plasticity induction (103% ± 7%, Δt = 6 ms). To test whether t-LTP was dependent on postsynaptic Ca^{2+} signals, we loaded cells with the Ca^{2+} chelator BAPTA (5 mM) through the recording pipette. Chelating intracellular Ca^{2+} completely abolished synaptic potentiation (98% ± 5%, Fig. 1*C*). These results are consistent with the idea that Ca^{2+} influx through NMDARs provided a trigger signal for the induction of synaptic plasticity. The narrow time window for t-LTP induction, however, was not consistent with the slow unbinding of glutamate from NMDARs (13).

AMPA Receptors Control the Temporal Window for t-LTP Induction. AMPARs mediate the majority of excitatory synaptic transmission in the vertebrate brain, and changes in the number of postsynaptic AMPARs are considered a major mechanism for the *expression* of different forms of long-term plasticity, including t-LTP (14). To test whether AMPAR activity is also required for the *induction* of t-LTP during pairing, we developed a protocol to transiently block these receptors. Bath application of 1 μM NBQX (2,3-Dioxo-6-nitro-1,2,3,4-tetrahydrobenzoquinoxaline -7-sulfonamide, subsaturating concentration) reduced AMPAR currents to 13% ± 2% (Fig. 2*A*). To test whether AMPAR inhibition was reversible, we washed the preparation with standard artificial (A)CSF while monitoring the

Author contributions: N.H., Å.G., and T.G.O. designed research; N.H., Å.G., and J.S.W. performed research; N.H., Å.G., J.S.W., and T.G.O. analyzed data; and N.H., Å.G., and T.G.O. wrote the paper.

The authors declare no conflict of interest.

This article is a PNAS Direct Submission.

Data deposition: Data have been deposited with the Model database of NEURON, http://senselab.med.yale.edu/modeldb/ (accession no. 116769).

[1]N.H. and Å.G. contributed equally to this work.

[2]To whom correspondence should be addressed. E-mail: thomas.oertner@fmi.ch.

This article contains supporting information online at www.pnas.org/lookup/suppl/doi:10.1073/pnas.1004562107/-/DCSupplemental.

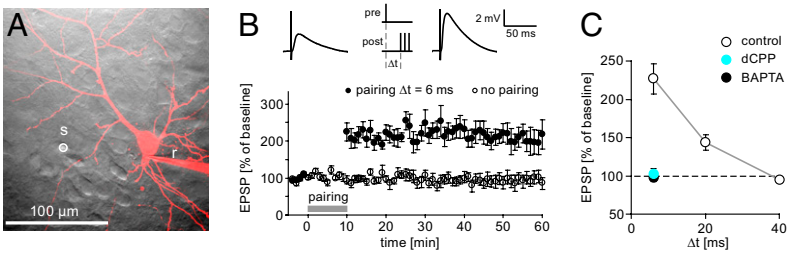

Fig. 1. Timing dependence of t-LTP. (*A*) Recording configuration, showing the tip of the stimulation electrode (s) and recording pipette (r) on a CA1 pyramidal cell. (*B*) Pairing of EPSPs with three postsynaptic APs (100 Hz) induced robust t-LTP (Δt = 6 ms, n = 7). In control experiments without pairing, EPSP amplitudes did not change (n = 7). Example traces show EPSPs before and 30 min after the pairing protocol. (*C*) t-LTP was sensitive to the relative timing between EPSP and postsynaptic firing (Δt = 6, 20, and 40 ms; n = 7, 7, and 6). The NMDA receptor antagonist dCPP (20 µM, n = 3) and the calcium chelator BAPTA (5 mM, n = 3) blocked t-LTP.

amplitude of postsynaptic responses. After 40 min of washout, EPSP amplitudes reached similar amplitudes as in control experiments without NBQX application (NBQX, 105% ± 12%; control, 96% ± 16%; Fig. 2 *A* and *B*). Having established that a subsaturating concentration of NBQX could be used to reversibly block AMPAR currents, we tested the effect of partial AMPAR block during pairing of pre- and postsynaptic activity. Reducing AMPAR currents during pairing blocked the induction of t-LTP at all tested time intervals (Fig. 2 *C* and *D*), demonstrating that AMPAR function was essential for t-LTP induction. At Δt = 20 ms, significant synaptic depression was observed after washout of NBQX (Fig. 2*D*). Pharmacological block of AMPAR function could potentially affect the integration of new receptors into the synapse. Therefore, we tested whether we could "rescue" LTP in NBQX by somatic current injection. Clamping the soma to the reversal potential of synaptic currents restored LTP induction in NBQX (Fig. S1), indicating that the essential function of AMPAR during t-LTP induction is indeed to provide depolarization. To further test how amplitude and duration of AMPAR-mediated EPSPs influences the temporal window for plasticity induction, we bath applied cyclothiazide (CTZ) to reduce AMPAR desensitization. Wash-in of CTZ (100 µM) resulted in EPSPs of larger amplitude (229% ± 47% of baseline) and duration (Fig. S2). In the continuous presence of CTZ, we could record stable EPSPs for >50 min (Fig. S2). Next, we paired pre- and postsynaptic activity in the presence of CTZ. At Δt = 40 ms, where no t-LTP was induced under control conditions, pairing in the presence of CTZ induced a lasting increase of EPSP amplitude to 157% ± 35% of baseline (Fig. 2 *E* and *F*), indicating that the permissive time window for t-LTP induction was broadened. At Δt = 20 ms, t-LTP was also significantly enhanced (190% ± 18%), whereas at Δt = 6 ms, t-LTP was similar to control conditions (241% ± 36%, Fig. 2*F*). Taken together, these results demonstrate that AMPARs not only are critical for the *expression*, but also control the *induction* of t-LTP.

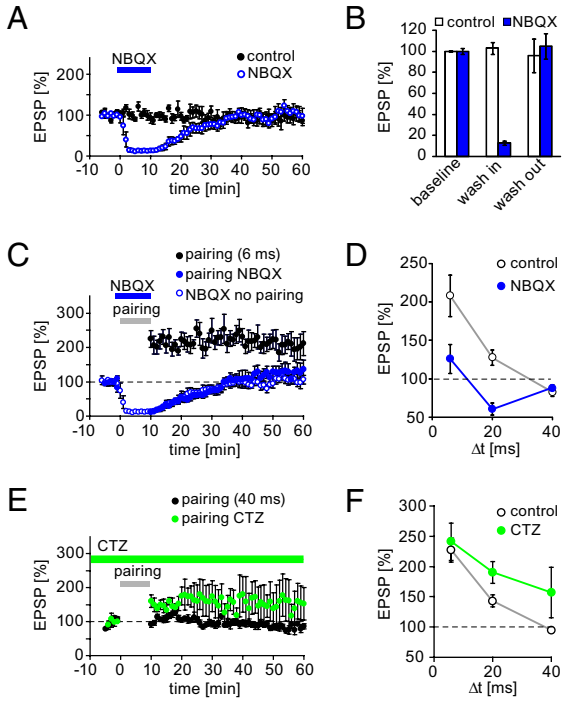

Fig. 2. t-LTP induction depends on AMPA receptor function. (*A*) Time course of EPSP amplitudes under control conditions (n = 7) and during wash-in and washout of NBQX (1 µM, n = 6). (*B*) Fifty to 60 min after the end of NBQX application, EPSPs reached 105% of baseline, not different from control experiments without drug application. (*C*) Time course of EPSP amplitude in pairing experiments (Δt = 6 ms) in the presence (n = 6) or absence (n = 7) of NBQX during the induction protocol. (*D*) Long-term plasticity after pairing under control conditions (n = 7, 6, and 6) and in NBQX (n = 6, 5, and 5). EPSPs were averaged 50–60 min after pairing. (*E*) Time course of EPSP amplitude in pairing experiments (Δt = 40 ms) under control conditions (n = 7) and in the presence of CTZ (100 µM, n = 4). Without pairing, the presence of CTZ did not induce plasticity (n = 4). (*F*) In the presence of CTZ (n = 4, 4, and 4), the window for t-LTP induction was extended to 40 ms.

Spine Ca^{2+} Transients During Pairing Stimulation Are Sensitive to Timing. Most AMPARs on CA1 pyramidal neurons contain GluR2 subunits that render them Ca^{2+} impermeable (15, 16). Thus, their strong effect on plasticity induction was rather surprising. We speculated that AMPARs might gate the Ca^{2+}-permeable and voltage-sensitive NMDARs through postsynaptic depolarization. To test this hypothesis, we measured postsynaptic Ca^{2+} signals in single dendritic spines using ratiometric two-photon imaging (17). CA1 pyramidal cells were filled with a mixture of a green Ca^{2+}-sensitive dye (Fluo 5F, 600 µM) and a volume-filling red dye (Alexa-Fluor 594, 30 µM). To prevent store-related Ca^{2+} nonlinearities, thapsigargin (10 µM) was added to the ACSF. Individual synapses on oblique dendrites (distance from soma: 90–150 µm) were stimulated by two-photon uncaging of 4-Methoxy-7-nitroindolinyl-caged-L-glutamate (MNI-glutamate, Fig. 3*A*) (18, 19). To ensure equal stimulation in all experiments, we adjusted the power of uncaging laser pulses to bleach 40–50% of the red dye in the focal plane (Fig. S3) (20). Under these conditions, the amplitude of uncaging-evoked currents (uEPSCs) was comparable to that of miniature EPSCs. Calcium imaging was performed under current clamp conditions. A small (<60 pA) negative holding current was applied in some experiments to keep the somatic membrane potential close to V_m = −65 mV. Spine Ca^{2+} transients were measured in response to glutamate uncaging alone, bAPs alone (three bAPs at 100 Hz, as in t-LTP experiments), and uncaging paired with bAPs at three different time intervals (Fig. 3 *B* and *C*). Pairing of glutamate uncaging

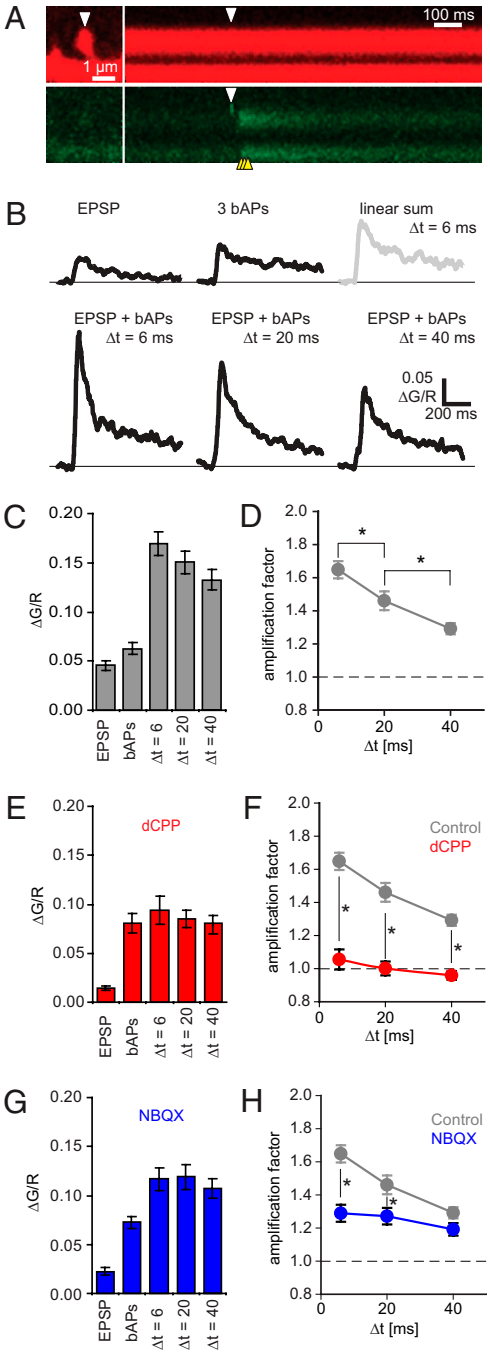

Fig. 3. Spine calcium transients during pairing stimulation. (*A*) Individual spines were stimulated by two-photon glutamate uncaging (white arrowhead). Ca^{2+} imaging was performed using line scans. (*Right*) *x*/*t* plot during pairing of uncaging (white arrowhead) with three bAPs (yellow arrowheads). Red, Alexa Fluor 594 (morphology); green, Fluo-5F. (*B*) Spine Ca^{2+} transients in response to uncaging alone, bAPs alone, and uncaging paired with bAPs at three different time intervals (Δt = 6, 20, and 40 ms). Traces are average responses from spine shown in *A*. The linear sum was calculated as the sum of the Ca^{2+} signal evoked by uncaging alone and the signal evoked by bAPs alone. (*C*) Peak Ca^{2+} amplitudes in response to uncaging alone, bAPs, or uncaging paired with bAPs (Δt = 6, 20, and 40 ms; n = 18). (*D*) Ca^{2+} transient amplitudes for different spike timings normalized by the linear sum. Ca^{2+} amplification was significantly different for different spike timings. (*E*) Spine Ca^{2+} transients with blocked NMDARs (20 µM dCPP, n = 9). (*F*) NMDAR block abolished Ca^{2+} amplification during pairing at all tested timings. (*G*) Spine Ca^{2+} transients with blocked AMPARs (10 µM NBQX, n = 18). (*H*) AMPAR block significantly reduced Ca^{2+} amplification at Δt = 6 and 20 ms.

with bAPs resulted in Ca^{2+} transients that were considerably larger than expected from a linear summation of the components. We quantified Ca^{2+} signal amplification by dividing the amplitude of measured Ca^{2+} transients by the expected Ca^{2+} transient amplitude (linear summation of components). The amplification factor was highly sensitive to the exact timing of correlated activity (linearity at Δt = 6 ms, 165% ± 5%; at Δt = 20 ms, 146% ± 6%; at Δt = 40 ms, 129% ± 3%, Fig. 3*D*). In addition, we monitored Ca^{2+} in the parent dendrite close (<2 µm) to the stimulated spine. In the dendrite, Ca^{2+} amplification was strongly reduced, indicating that highly supralinear Ca^{2+} signals were generated locally in the spine heads (Fig. S4). The sensitivity of spine head Ca^{2+} signals to the relative timing of glutamate transient and postsynaptic depolarization suggested that they could act as an instructive signal for t-LTP.

Synergy Between AMPARs, NMDARs, and Back-Propagating APs. To test whether Ca^{2+} supralinearity was dependent on NMDAR activity, we pharmacologically blocked these receptors by dCPP (20 µM, Fig. 3*E*). Blockade of NMDARs did not affect the amplitude of uEPSCs, but significantly depressed uncaging-evoked Ca^{2+} transients (Fig. S5), demonstrating that NMDARs are a major pathway for Ca^{2+} entry during synaptic activity, but contributed little to postsynaptic depolarization. In pairing experiments, blockade of NMDARs abolished Ca^{2+} supralinearity for all tested timings (Fig. 3*F*), confirming that NMDAR activity was *necessary* for the conversion of spike timings to supralinear Ca^{2+} signals of different amplitudes. To test whether direct interaction between NMDARs and bAPs was *sufficient* to generate supralinear Ca^{2+} transients, we next blocked AMPARs (NBQX, 10 µM; Fig. 3*G*). Interestingly, this manipulation strongly reduced Ca^{2+} amplification at Δt = 6 and 20 ms, but had little effect at Δt = 40 ms (Fig. 3*H*). The remaining amplification likely reflects direct unblocking of NMDARs by bAPs, since its timing dependence was weak and consistent with NMDAR kinetics (13). Blockade of AMPARs also strongly reduced the absolute amplitude of uncaging-evoked spine Ca^{2+} transients, providing further evidence that NMDARs were gated by AMPAR-mediated depolarization during synaptic activity (Fig. S5). Together, these results suggest that NMDARs interact with bAPs to generate supralinear Ca^{2+} transients and that this amplification is significantly enhanced by AMPARs in the critical window permissive for t-LTP.

Amplification of Spine Ca^{2+} Signals Depends on Degree of Isolation from Dendrite. In previous studies, we and others have shown that spine head depolarization is strongest in spines that are well isolated from the dendrite (21–23). Because the results of our t-LTP experiments suggested that the precision of coincidence detection depends on EPSP amplitude, we expected well-isolated spines to be most sensitive to pairing stimulation. The diffraction-limited performance of our two-photon microscope did not allow resolving the precise geometry of spine necks optically. Instead, we used fluorescence recovery after photobleaching (FRAP) to estimate the diffusional coupling between individual spines and dendrites (Fig. 4*A*). Indeed, during pairing stimulation at Δt = 6 ms, amplification of spine Ca^{2+} transients was strongest in spines with long FRAP time constants, indicative of weak coupling (Fig. 4 *B* and *C*). No correlation of Ca^{2+} signals with FRAP time constants was found for longer pairing intervals (Fig. 4*D*) or in pairing experiments under AMPAR or NMDAR block (Fig. 4 *E* and *F*). Because the range of time constants in acute slices was narrow (range: 15–150 ms), we repeated the pairing experiments in hippocampal slice cultures (range: 21–332 ms, Fig. S6). At Δt = 5 ms, amplification of spine Ca^{2+} transients was strongly correlated with FRAP time constants (R = 0.681, P = 0.001). Consistent with our results from acute slices, there was no correlation at Δt = 50 ms in organotypic cultures (R = 0.056, P = 0.823). These

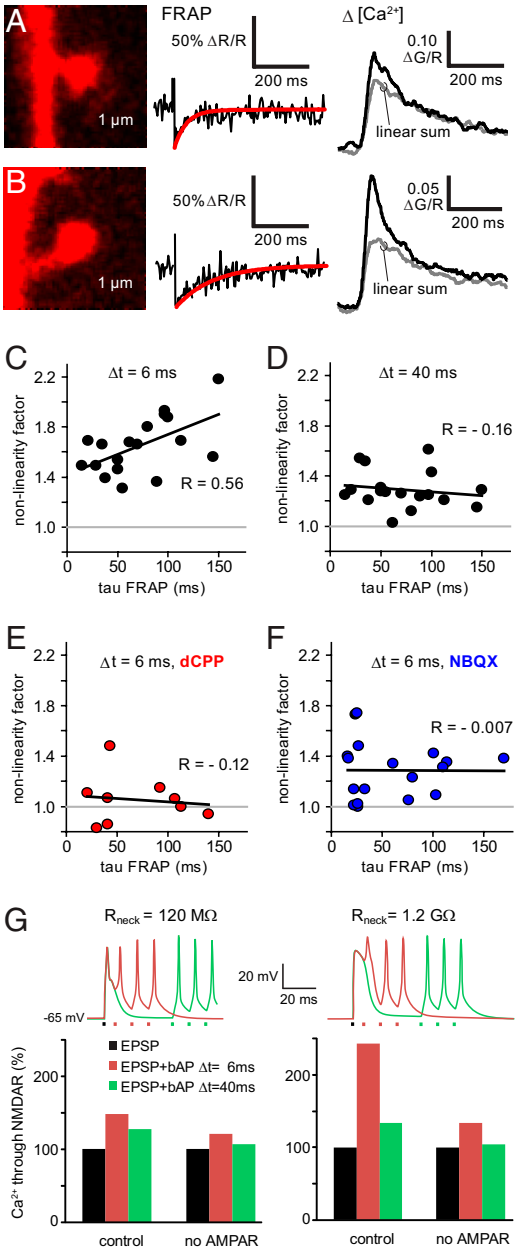

Fig. 4. Correlations between calcium nonlinearity and diffusional coupling of spines. (*A*) At individual spines, Ca^{2+} transients during pairing were measured. Before and after pairing, fluorescence recovery after photobleaching (FRAP) was used to quantify diffusional coupling. (*B*) Example of a well-isolated spine. (*C*) At Δt = 6 ms, the amount of Ca^{2+} signal amplification was correlated with FRAP time constants (n = 18). (*D*) At Δt = 40 ms, no correlation was observed (n = 18). (*E*) Blocking NMDARs with dCPP (20 μM) abolished Ca^{2+} signal amplification in all spines (Δt = 6 ms, n = 9). (*F*) Blocking AMPARs with NBQX (10 μM) reduced Ca^{2+} signal amplification. No correlation with FRAP time constants was observed (Δt = 6 ms, n = 18). (*G*) Modeling coincidence detection in spines with NEURON. In a spine with a low resistance neck (*Left*), Ca^{2+} influx through NMDARs is slightly enhanced (148% of EPSP alone) by three bAPs arriving 6 ms after the EPSP. Traces shows the membrane potential in the spine head for paring at 6 ms (red) and at 40 ms (green). In a spine with high neck resistance (*Right*), Ca^{2+} is dramatically amplified at Δt = 6 ms (243% of EPSP alone). The corresponding voltage trace (red) shows significant broadening of the EPSP in the spine head by the first bAP. Removal of AMPARs from the simulation reduces Ca^{2+} amplification to 134%.

data support the idea that the synergistic interaction between AMPA currents, bAPs, and NMDARs is a local electrical phenomenon that works best in spines that have some degree of isolation from the dendrite.

Modeling Coincidence Detection with NEURON. To test our notion that electrical compartmentalization in spines is crucial for coincidence detection, we used a previously published model of a CA1 pyramidal cell spine equipped with AMPA and NMDA receptors and voltage-gated Ca^{2+} channels (21). Spine channel densities were not modified, but active conductances (Hodgkin–Huxley) were added to somatic and dendritic compartments to simulate bAPs. The model was run with two different spine neck diameters, corresponding to 120 MΩ and 1.2 GΩ resistances. We monitored Ca^{2+} currents through NMDARs as well as the membrane potential in the spine head for two different pairings (Δt = 6 and 40 ms; Fig. 4*G*). High Ca^{2+} nonlinearity (243%) was found *only* in the spine with a high resistance neck and *only* at Δt = 6 ms. When we removed AMPARs from the simulation, nonlinearity was reduced to 133%, consistent with experiments in NBQX (Fig. 4*F*). The modeling results indicate that electrical compartmentalization in spines can account for the correlation between diffusion time constants and calcium amplification that we observed in our experiments. Furthermore, the model allowed us to inspect the voltage in the spine head and revealed a considerable broadening of the EPSP for Δt = 6 ms (Fig. 4*G*), providing an explanation for the efficient unblocking of NMDARs under these conditions.

Discussion

Ca^{2+} transients in dendritic spines during pairing of pre- and postsynaptic activity are highly nonlinear; i.e., their amplitude exceeds the sum of Ca^{2+} transients caused by synaptic activation and by back-propagating APs alone (24). We show that these Ca^{2+} transients depend on simultaneous activation of NMDA and AMPARs and are highly sensitive to the relative timing of glutamate receptor activation and bAP arrival, suggesting that Ca^{2+} transients encode timing information and could serve as an instructive signal for plasticity induction. In the absence of AMPA receptor currents, Ca^{2+} signals were still supralinear, but the sharp sensitivity to timing was lost. Interestingly, not all spines displayed the same nonlinear enhancement of Ca^{2+} influx: Spines that were diffusionally isolated from the dendrite had the highest amplification factor during pairing stimulation, indicating that the precision of coincidence detection is not the same at all synapses. We could reproduce the amplification of Ca^{2+} currents in numerical simulations where we varied the spine neck diameter to simulate stronger and weaker coupling to the dendrite.

Although the dependence of postsynaptic Ca^{2+} influx during the EPSP on AMPAR function has been described in previous studies (9, 21, 22, 24), the impact of the AMPA-EPSP on the precision of coincidence detection has not been directly shown. Our Ca^{2+} imaging data suggest that AMPARs critically boost the nonlinear interaction between NMDAR currents and back-propagating APs in a narrow time window of ~20 ms, reminiscent of the sharp window where t-LTP can occur. The effect of the AMPAR-mediated EPSP can be described as a *sensitization* of the entire spine to additional depolarization: The IV curve of NMDARs for Ca^{2+} reaches its maximum slope at membrane potentials between −30 and −20 mV (21). CaV2.3 channels, another important source of Ca^{2+} in spines, have a similar activation curve (25). If a spine head is depolarized to this potential, a brief additional depolarization by a bAP will have dramatic effects on local Ca^{2+} currents. Milliseconds later, when the AMPAR current is shut off and spine depolarization has decayed, the same bAP is largely ineffective in unblocking NMDARs (Fig. 4*G*). Recent estimates from voltage imaging experiments have confirmed high-amplitude EPSPs in spines and a steep voltage drop along the spine neck (23, 26). Alternative

mechanisms for a narrow t-LTP window, such as boosting of AP back-propagation by inactivation of K^+ channels, have been proposed (27, 28). However, because AP boosting is thought to require the simultaneous activation of many excitatory synapses and affects coincidence detection mostly in the distal portion of the dendritic tree, it is not likely to have a strong effect under our experimental conditions.

In our experiments, the time window for plasticity induction was narrower than the window for Ca^{2+} supralinearity (Figs. 1*C* and 3*D*). However, several factors have to be taken into account when relating optically measured Ca^{2+} signals to plasticity induction. First, the peak amplitude of free Ca^{2+} transients in our imaging experiments was blunted by the addition of Ca^{2+}-sensitive dye (29). Under physiological conditions, in the absence of exogenous Ca^{2+} buffer, we expect an even steeper dependence of Ca^{2+} transient amplitude on timing. Because optical Ca^{2+} measurements interfere with the concentration of free Ca^{2+} ions inside the cell and thus affect plasticity induction, we chose to investigate Ca^{2+} transient amplitude and t-LTP in separate experiments. Second, postsynaptic Ca^{2+} transients trigger plasticity through a series of biochemical reactions, and the relation between bulk Ca^{2+} concentration ($[Ca^{2+}]$) and potentiation is known to be nonlinear (30, 31). Compared with the $[Ca^{2+}]$ reported by the Ca^{2+}-sensitive dye, fast endogenous Ca^{2+} sensors such as calmodulin will sense much higher local $[Ca^{2+}]$ close to open NMDARs (32). Dependent on the head volume of each individual spine, these local Ca^{2+} domains will be more or less diluted before we can detect any fluorescence increase in the spine. In accordance, when we compared our electrophysiological and imaging experiments, we found a correlation between spine Ca^{2+} transient amplitudes ($\Delta G/R$) and the amount of spike-timing-dependent plasticity (STDP) induced by the equivalent stimulation protocol ($R = 0.859$, $P = 0.029$). When we considered Ca^{2+} amplification factors rather than absolute $[Ca^{2+}]$, the significance of the correlation with STDP increased notably ($R = 0.930$, $P = 0.007$, Fig. 5). How could a Ca^{2+}-sensing molecule like calmodulin calculate a derived value such as the Ca^{2+} amplification factor? One possibility is that high amplification factors indicate a high degree of NMDAR unblocking during pairing and thus reflect the occurrence of many Ca^{2+} nanodomains in the postsynaptic density, independent of later dilution in the spine cytoplasm. Thus, a Ca^{2+} sensor in the spine would not have to calculate the nonlinearity factor; it simply has to be located very close to the influx channels.

Consistent with previous reports (33, 34), we found that pharmacologically induced changes in EPSP amplitude and waveform altered the permissive window for t-LTP. This result suggests that neurons could actively modify their sensitivity to STDP by changing AMPAR gating properties, for example, by altering subunit composition or accessory proteins (35–37). Consistent with this idea, other channels regulating amplitude and duration of postsynaptic depolarization, such as voltage-dependent K^+ or Ca^{2+} channels, have also been reported to affect the window for plasticity induction (21, 33, 38, 39). A second endogenous mechanism that is known to affect spine head depolarization is activity-dependent changes in diffusional coupling (18, 21). In spines of both acute slices and organotypic cultures, we found significant correlations between diffusional isolation and the degree of Ca^{2+} nonlinearity (Fig. 4*B* and Fig. S6), but only for rapid uEPSP-bAP pairings ($\Delta t = 5$ or 6 ms). In spines weakly isolated from the dendrite, we still found some residual Ca^{2+} amplification (20–30%, Fig. S6), similar to spines under AMPAR block (Fig. 3*G*) and to the weak Ca^{2+} amplification seen in the dendrite (Fig. S4). Residual amplification can be readily explained by direct unblocking of NMDARs by bAPs. In well-isolated spines, we show that a Ca^{2+}-sensitive readout mechanism could sense the time lag between synaptic activation and postsynaptic spikes with the required temporal precision (Fig. 4*B*). Although we do not provide direct experimental evidence, it is quite likely that t-LTP (Fig. 1) was induced primarily at these well-isolated spine synapses. In summary, AMPARs not only mediate the majority of excitatory transmission in the vertebrate brain, but also play a key role in the induction of associative synaptic plasticity. The ability of synapses to measure coincidence with millisecond precision cannot be explained by the gating properties of NMDARs alone, but is a consequence of the strong and confined depolarization of the spine head during the EPSP.

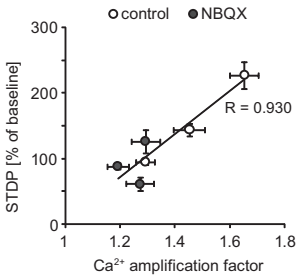

Fig. 5. The degree of amplification of spine calcium transients was correlated with the amount of STDP induced by the same protocol ($\Delta t = 6$, 20, and 40 ms; $P = 0.007$). Blocking AMPARs (gray markers) reduced Ca^{2+} amplification and prevented t-LTP induction.

Methods

Slice Preparation. Acute hippocampal brain slices were prepared from Wistar rats (postnatal days 14–19). Horizontal slices (350 μm thick) were cut on a vibroslicer (Leica) in ice-cold solution containing 110 mM choline chloride, 25 mM $NaHCO_3$, 25 mM D-glucose, 11.6 mM sodium ascorbate, 7 mM $MgSO_4$, 2.5 mM KCl, 1.25 mM NaH_2PO_4, and 0.5 mM $CaCl_2$. Slices were incubated at 34 °C for 30 min in oxygenated ACSF, containing 127 mM NaCl, 25 mM $NaHCO_3$, 25 mM D-glucose, 2.5 mM KCl, 1 mM $MgCl_2$, 2 mM $CaCl_2$, and 1.25 mM NaH_2PO_4, and then stored at room temperature until used. For whole-cell recordings, the ACSF was supplemented with 10 μM bicuculline and 30 μM serine. For uncaging experiments, we added MNI-glutamate (5 mM) and thapsigargin (10 μM) to prevent store-dependent Ca^{2+} nonlinearities. In a subset of experiments, we added NBQX (1 or 10 μM) to block AMPARs, dCPP (20 μM) to block NMDARs, or cyclothiazide (100 μM) to reduce AMPAR desensitization.

Electrophysiology. Current-clamp recordings from CA1 pyramidal cells were performed at 30 °C, using a Multiclamp 700B amplifier (Axon Instruments) and 5–8 MΩ pipettes filled with 135 mM K-gluconate, 10 mM Hepes, 10 mM sodium phosphocreatine, 3 mM sodium ascorbate, 4 mM $MgCl_2$, 4 mM Na2-ATP, 0.4 mM Na-GTP, and 0.03 mM Alexa-Fluor 594 (pH 7.2, 295 mOsm). For Ca^{2+} imaging experiments, 0.6 mM Fluo 5F was added to the intracellular solution (Molecular Probes; $K_d \sim 0.8$ μM). A monopolar stimulation electrode filled with 1 M NaCl was positioned 15–25 μm from an oblique dendrite (150–200 μm from the soma), using laser DIC. A brief hyperpolarizing pulse (0.2 ms, −2 to −5 V) was delivered by a stimulus isolator (NPI Electronics) to stimulate Schaffer collaterals at 0.1 Hz. Recorded pyramidal cells had resting membrane potentials of −66 mV ± 1 mV and input resistances of 190 ± 89 MΩ ($n = 55$ cells). Recordings were discarded if input or series resistance changed by >30% during the experiment. LTP was induced by 120 pairings of a single evoked EPSP with three postsynaptic APs (at 100 Hz) at 0.2 Hz. To compensate for the delay between extracellular stimulation pulse and somatic EPSP, we adjusted the timing of the postsynaptic AP burst for each recorded cell, using the test pulses during baseline to quantify EPSP delay. The time interval between the EPSP and the postsynaptic APs (Δt) was defined as the time between the onset of the EPSP at the soma (50% of EPSP peak) and the onset of the somatic current injection (2 ms) that triggered the first AP. The amount of potentiation was assessed 25–35 min after the beginning of the induction protocol and expressed as percentage of the baseline EPSP amplitude. In NBQX washout experiments, the amount of potentiation was measured 50–60 min after induction.

Two-Photon Laser Scanning Microscopy and Glutamate Uncaging. We used a custom-built two-photon imaging and uncaging setup based on an Olympus BX51WI microscope equipped with a LUMFL 60× 1.1-NA objective.

Two ultrafast IR lasers (Chameleon-Ultra; Coherent) controlled by Pockel's cells (350-80; Conoptics) were combined for two-photon imaging (810 nm) and uncaging of MNI-glutamate (730 nm). Fluorescence was detected in epi- and transfluorescence modes, using four photomultiplier tubes (R3896; Hamamatsu). To measure Ca^{2+} signals, green (Fluo 5F) and red (Alexa-Fluor 594) fluorescence was collected during 250-Hz line scans across the spine head and its parent dendrite. Calcium imaging was performed in a current clamp. Glutamate uncaging was achieved using a 0.5-ms laser pulse focused ~0.5 μm off the spine center, in a direction away from the parent dendrite. Laser intensity was ~50 mW measured in the back focal plane of the objective. Fluorescence changes for the different stimulation protocols were quantified as increase in green fluorescence (ΔG) normalized to the average red fluorescence ($\Delta G/R$) (17). Photomultiplier dark noise was subtracted. To quantify Ca^{2+} transient amplitudes for each spine, peak $\Delta G/R$ was averaged over 5–10 trials for each stimulation protocol. The linearity of Ca^{2+} transients was calculated by dividing the peak Ca^{2+} transient amplitude for a given pairing protocol by the expected peak amplitude (the linear sum) of uncaging-evoked and bAP-evoked Ca^{2+} transients. Data are reported as mean ± SEM. To test for significance, we used the Mann–Whitney rank sum test or the Wilcoxon signed-rank test at a significance level of $P = 0.05$.

Compartmental Modeling. Our compartmental model of a CA pyramidal cell spine is publicly available at the NEURON model database (http://senselab.med.yale.edu/modeldb/; accession no. 116769). For a detailed description, see Grunditz et al. (21).

ACKNOWLEDGMENTS. We thank D. Gerosa for excellent technical assistance and A. Lüthi and R. W. Friedrich for critically reading the manuscript. This work was supported by the Novartis Research Foundation, SystemsX.ch, and the Gebert Rüf Foundation.

1. Markram H, Lübke J, Frotscher M, Sakmann B (1997) Regulation of synaptic efficacy by coincidence of postsynaptic APs and EPSPs. *Science* 275:213–215.
2. Bi GQ, Poo MM (1998) Synaptic modifications in cultured hippocampal neurons: Dependence on spike timing, synaptic strength, and postsynaptic cell type. *J Neurosci* 18:10464–10472.
3. Zhang LI, Tao HW, Holt CE, Harris WA, Poo M (1998) A critical window for cooperation and competition among developing retinotectal synapses. *Nature* 395:37–44.
4. Hebb DO (1949) *The Organization of Behavior* (Wiley, New York).
5. Song S, Miller KD, Abbott LF (2000) Competitive Hebbian learning through spike-timing-dependent synaptic plasticity. *Nat Neurosci* 3:919–926.
6. Rubin JE, Gerkin RC, Bi GQ, Chow CC (2005) Calcium time course as a signal for spike-timing-dependent plasticity. *J Neurophysiol* 93:2600–2613.
7. Bender VA, Bender KJ, Brasier DJ, Feldman DE (2006) Two coincidence detectors for spike timing-dependent plasticity in somatosensory cortex. *J Neurosci* 26:4166–4177.
8. Koester HJ, Sakmann B (1998) Calcium dynamics in single spines during coincident pre- and postsynaptic activity depend on relative timing of back-propagating action potentials and subthreshold excitatory postsynaptic potentials. *Proc Natl Acad Sci USA* 95:9596–9601.
9. Yuste R, Majewska A, Cash SS, Denk W (1999) Mechanisms of calcium influx into hippocampal spines: Heterogeneity among spines, coincidence detection by NMDA receptors, and optical quantal analysis. *J Neurosci* 19:1976–1987.
10. Sjöström PJ, Rancz EA, Roth A, Häusser M (2008) Dendritic excitability and synaptic plasticity. *Physiol Rev* 88:769–840.
11. Higley MJ, Sabatini BL (2008) Calcium signaling in dendrites and spines: Practical and functional considerations. *Neuron* 59:902–913.
12. Oertner TG (2009) How do synapses measure milliseconds? *Front Comput Neurosci* 3:7.
13. Kampa BM, Clements J, Jonas P, Stuart GJ (2004) Kinetics of Mg2+ unblock of NMDA receptors: Implications for spike-timing dependent synaptic plasticity. *J Physiol* 556: 337–345.
14. Malinow R, Malenka RC (2002) AMPA receptor trafficking and synaptic plasticity. *Annu Rev Neurosci* 25:103–126.
15. Lu W, et al. (2009) Subunit composition of synaptic AMPA receptors revealed by a single-cell genetic approach. *Neuron* 62:254–268.
16. Wenthold RJ, Petralia RS, Blahos J II, Niedzielski AS (1996) Evidence for multiple AMPA receptor complexes in hippocampal CA1/CA2 neurons. *J Neurosci* 16:1982–1989.
17. Yasuda R, et al. (2004) Imaging calcium concentration dynamics in small neuronal compartments. *Sci STKE* 2004:pl5.
18. Bloodgood BL, Sabatini BL (2005) Neuronal activity regulates diffusion across the neck of dendritic spines. *Science* 310:866–869.
19. Matsuzaki M, et al. (2001) Dendritic spine geometry is critical for AMPA receptor expression in hippocampal CA1 pyramidal neurons. *Nat Neurosci* 4:1086–1092.
20. Bloodgood BL, Sabatini BL (2007) Nonlinear regulation of unitary synaptic signals by CaV(2.3) voltage-sensitive calcium channels located in dendritic spines. *Neuron* 53: 249–260.
21. Grunditz A, Holbro N, Tian L, Zuo Y, Oertner TG (2008) Spine neck plasticity controls postsynaptic calcium signals through electrical compartmentalization. *J Neurosci* 28: 13457–13466.
22. Bloodgood BL, Giessel AJ, Sabatini BL (2009) Biphasic synaptic Ca influx arising from compartmentalized electrical signals in dendritic spines. *PLoS Biol* 7:e1000190.
23. Araya R, Jiang J, Eisenthal KB, Yuste R (2006) The spine neck filters membrane potentials. *Proc Natl Acad Sci USA* 103:17961–17966.
24. Nevian T, Sakmann B (2004) Single spine Ca2+ signals evoked by coincident EPSPs and backpropagating action potentials in spiny stellate cells of layer 4 in the juvenile rat somatosensory barrel cortex. *J Neurosci* 24:1689–1699.
25. Foehring RC, Mermelstein PG, Song WJ, Ulrich S, Surmeier DJ (2000) Unique properties of R-type calcium currents in neocortical and neostriatal neurons. *J Neurophysiol* 84: 2225–2236.
26. Palmer LM, Stuart GJ (2009) Membrane potential changes in dendritic spines during action potentials and synaptic input. *J Neurosci* 29:6897–6903.
27. Watanabe S, Hoffman DA, Migliore M, Johnston D (2002) Dendritic K+ channels contribute to spike-timing dependent long-term potentiation in hippocampal pyramidal neurons. *Proc Natl Acad Sci USA* 99:8366–8371.
28. Migliore M, Hoffman DA, Magee JC, Johnston D (1999) Role of an A-type K+ conductance in the back-propagation of action potentials in the dendrites of hippocampal pyramidal neurons. *J Comput Neurosci* 7:5–15.
29. Maravall M, Mainen ZF, Sabatini BL, Svoboda K (2000) Estimating intracellular calcium concentrations and buffering without wavelength ratioing. *Biophys J* 78:2655–2667.
30. Lisman JE, Zhabotinsky AM (2001) A model of synaptic memory: A CaMKII/PP1 switch that potentiates transmission by organizing an AMPA receptor anchoring assembly. *Neuron* 31:191–201.
31. Nevian T, Sakmann B (2006) Spine Ca2+ signaling in spike-timing-dependent plasticity. *J Neurosci* 26:11001–11013.
32. Keller DX, Franks KM, Bartol TM, Jr, Sejnowski TJ (2008) Calmodulin activation by calcium transients in the postsynaptic density of dendritic spines. *PLoS ONE* 3:e2045.
33. Fuenzalida M, Fernandez de Sevilla D, Buño W (2007) Changes of the EPSP waveform regulate the temporal window for spike-timing-dependent plasticity. *J Neurosci* 27: 11940–11948.
34. Fuenzalida M, Fernández de Sevilla D, Couve A, Buño W (2010) Role of AMPA and NMDA receptors and back-propagating action potentials in spike timing-dependent plasticity. *J Neurophysiol* 103:47–54.
35. Mosbacher J, et al. (1994) A molecular determinant for submillisecond desensitization in glutamate receptors. *Science* 266:1059–1062.
36. Schwenk J, et al. (2009) Functional proteomics identify cornichon proteins as auxiliary subunits of AMPA receptors. *Science* 323:1313–1319.
37. Milstein AD, Zhou W, Karimzadegan S, Bredt DS, Nicoll RA (2007) TARP subtypes differentially and dose-dependently control synaptic AMPA receptor gating. *Neuron* 55:905–918.
38. Ngo-Anh TJ, et al. (2005) SK channels and NMDA receptors form a Ca2+-mediated feedback loop in dendritic spines. *Nat Neurosci* 8:642–649.
39. Humeau Y, et al. (2005) Dendritic spine heterogeneity determines afferent-specific Hebbian plasticity in the amygdala. *Neuron* 45:119–131.

Supporting Information

Holbro et al. 10.1073/pnas.1004562107

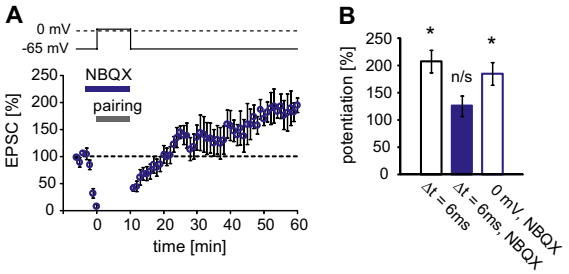

Fig. S1. Rescue of LTP in NBQX by somatic depolarization. (*A*) LTP could be induced in the presence of 1 μM NBQX if the cell was voltage clamped to the reversal potential of synaptic currents during pairing ($n = 6$). During baseline and washout, holding potential was −65 mV. To improve space clamp, a Cs^+-based intracellular solution was used consisting of 135 mM Cesium methanesulfonate, 10 mM Hepes, 4 mM $MgCl_2$, 4 mM Na_2-ATP, 0.4 mM Na-GTP, 10 mM Na-phosphocreatine, and 5 mM glutathione. LTP was induced when NBQX wash-in reached steady state by pairing 120 single EPSCs evoked at 0.2 Hz (equivalent to the spike-timing protocol) with constant postsynaptic depolarization to the synaptic reversal potential (0 V at the stimulated synapses, +8 to +12 mV at the soma). NBQX washout was started after completion of the LTP protocol. (*B*) Although NBQX blocked the induction of t-LTP in the current clamp, it did not prevent LTP induction in the voltage clamp at the reversal potential. Potentiation of the postsynaptic response relative to baseline in a time window of 50–60 min after onset of pairing is plotted for three experimental conditions.

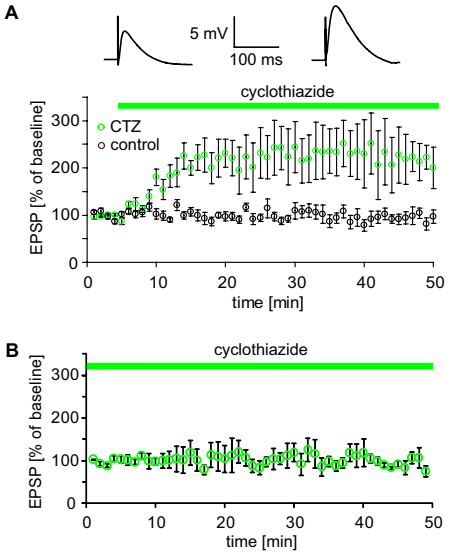

Fig. S2. Wash-in of cyclothiazide (CTZ). (*A*) Time course of EPSP amplitude in control condition (black, $n = 7$) and during wash-in of 100 μM CTZ (green, $n = 5$). Bath application of CTZ increases EPSP amplitude. Example traces show EPSPs before and 30 min after CTZ application. (*B*) Without pairing, the presence of CTZ did not induce plasticity ($n = 4$).

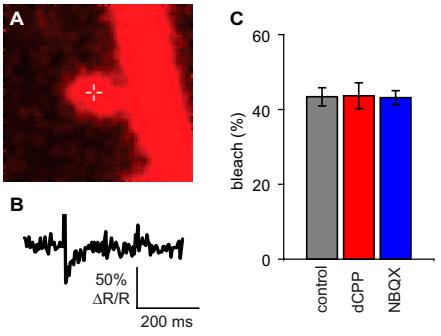

Fig. S3. Assessing local laser intensity by bleaching of fluorescent dye. (*A*) To ensure equal stimulation strenght in different experiments, we directed a laser pulse to the center of a spine and monitored the amount of bleaching of the red fluorophore (Alexa Fluor 594) before each set of calcium measurements. (*B*) Fluorescence recovery after photobleaching (FRAP) of the red fluorophore in spine shown in *A*. (*C*) Alexa Fluor 594 bleaching was similar under different pharmacological conditions, indicating identical stimulation strength ($n = 18$, 9, and 18).

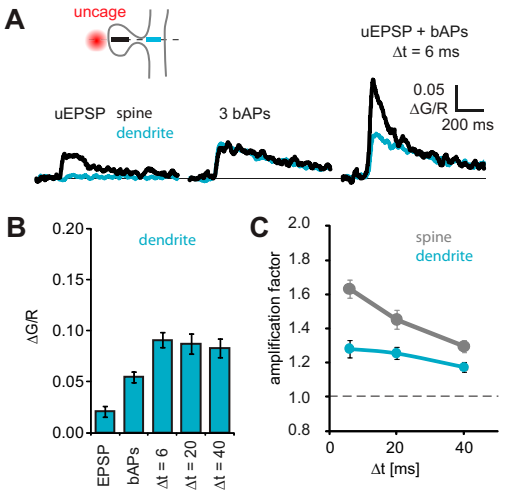

Fig. S4. Dendritic calcium transients during pairing stimulation. (*A*) Spine and dendritic Ca^{2+} transients in response to uncaging alone, bAPs alone, and uncaging paired with bAPs (Δt = 6 ms). Dendritic Ca^{2+} was measured close to the base of the spine. (*B*) Peak dendritic Ca^{2+} amplitudes in response to uncaging alone, bAPs alone, or uncaging paired with bAPs (Δt = 6, 20, and 40 ms; n = 16). (*C*) Spine and dendritic Ca^{2+} transient amplitudes for different spike timings normalized by the linear sum (n = 16). In the dendrite close to the stimulated spine, both the degree of Ca^{2+} amplification and the dependence on timing were strongly reduced.

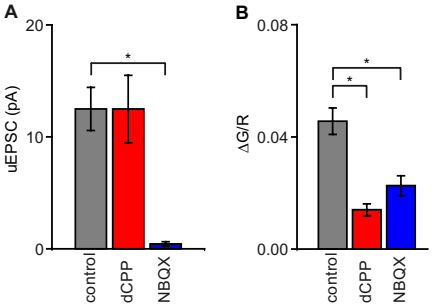

Fig. S5. Effect of glutamate receptor blockers on uncaging-evoked postsynaptic currents and calcium signals. (*A*) Blocking NMDARs with dCPP (20 μM) did not significantly affect uEPSCs. Blocking AMPARs with NBQX (10 μM) strongly reduced uEPSCs (n = 18, 9, and 18). (*B*) Blocking NMDARs with dCPP (20 μM) or AMPARs with NBQX (10 μM) significantly depressed uncaging-evoked spine calcium signals (n = 18, 9, and 18). *$P < 0.05$.

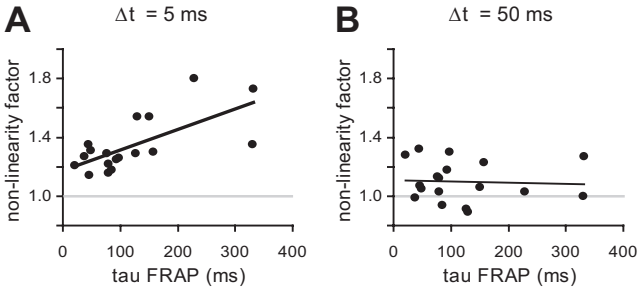

Fig. S6. Correlation between calcium nonlinearity and diffusional coupling of spines in organotypic slice cultures. Spines on oblique dendrites of CA1 pyramidal cells were stimulated by two-photon uncaging of MNI-glutamate and FRAP time constants were measured. (*A*) At Δt = 5 ms, the amount of Ca^{2+} signal amplification was correlated with FRAP time constants (R = 0.681, P = 0.001, n = 18). (*B*) At Δt = 50 ms, no correlation was observed (R = 0.056, P = 0.823, n = 18).